Engineering protein-specific proteases: targeting active RAS

Short title: Proteases for degrading active RAS

Yingwei Chen[a,1], Eric A. Toth[b,c,d,1], Biao Ruan[a,1], Eun Jung Choi[a], Richard Simmerman[a], Yihong Chen[b], Yanan He[b], Ruixue Wang[b], Raquel Godoy-Ruiz[b,d,i], Harlan King[b,e], Gregory Custer[b,f], D. Travis Gallagher[b,e], David A. Rozak[g], Melani Solomon[b,f], Silvia Muro[b,f,h], David J. Weber[b,c,d,i], John Orban[b,j,2], Thomas R. Fuerst[b,k,2], and Philip N. Bryan[a,b,2]

[a] Potomac Affinity Proteins, 11305 Dunleith Pl, North Potomac, MD 20878, USA

[b] Institute for Bioscience and Biotechnology Research, 9600 Gudelsky Drive Rockville, MD 20850, USA

[c] Marlene and Stewart Greenebaum Cancer Center, University of Maryland School of Medicine, Baltimore, Maryland 21201, USA.

[d] Center for Biomolecular Therapeutics, 9600 Gudelsky Drive Rockville, MD 20850, USA

[e] National Institute of Standards and Technology and the University of Maryland, 9600 Gudelsky Drive, Rockville Maryland 20850 USA

[f] Department of Bioengineering, University of Maryland, College Park, Maryland, 20742

[g] Unified Culture Collection, United States Army Research Institute of Infectious Diseases, 1425 Porter Street, Fort Detrick, MD 21702

[h] Institute for Bioengineering of Catalonia of the Barcelona Institute of Science and Technology & Institution of Catalonia for Research and Advanced Studies, Barcelona, Spain

[i] Department of Biochemistry and Molecular Biology, University of Maryland School of Medicine, Baltimore, Maryland 21201, USA.

[j] Department of Chemistry and Biochemistry, University of Maryland, College Park, Maryland, 20742

[k] Department of Cell Biology and Molecular Genetics, University of Maryland, College Park, Maryland 20742

[1] Chen, Toth, and Ruan contributed equally

[2] To whom correspondence may be addressed. email: pbryan@potomac-affinity-proteins.com, tfuerst@umd.edu, jorban@umd.edu
Proofs should be sent to: Philip Bryan
Potomac Affinity Proteins, 11305 Dunleith Pl, North Potomac, MD 20878, USA
pbryan@potomac-affinity-proteins.com
Tel: 240-252-9748

Key words: protein design, enzymology, cancer, structural biology

Abstract: We describe the design, kinetic properties, and structures of engineered subtilisin proteases that degrade the active form of RAS by cleaving a conserved sequence in switch 2. RAS is a signaling protein that, when mutated, drives a third of human cancers. To generate high specificity for the RAS target sequence, the active site was modified to be dependent on a cofactor (imidazole or nitrite) and protease sub-sites were engineered to create a linkage between substrate and cofactor binding. Selective proteolysis of active RAS arises from a 2-step process wherein sub-site interactions promote productive binding of the cofactor, enabling cleavage. Proteases engineered in this way specifically cleave active RAS *in vitro*, deplete the level of RAS in a bacterial reporter system, and also degrade RAS in human cell culture. Although these proteases target active RAS, the underlying design principles are fundamental and will be adaptable to many target proteins.

Engineering proteases that cleave specific signaling proteins in active conformations would open new possibilities to study, regulate, and reprogram signaling pathways (1). Our target here was the active state of the rat sarcoma (RAS) oncoprotein. RAS is a small GTPase that, in response to growth factors, activates downstream effector molecules such as those in the MAPK pathway and others, thereby driving pathways that stimulate cell growth. Three RAS isoforms (HRAS, KRAS, and NRAS) are the primary regulators of cell signaling pathways. All three isoforms coexist in cells and have distinct but overlapping roles in signaling (2, 3). Inherent to the function of RAS is a switch between its inactive (GDP-bound) and active (GTP-bound) forms. Two regions, termed switch 1 (amino acids 30-38) and switch 2 (amino acids 59-76), undergo structural changes as RAS cycles between the GDP-bound and GTP-bound forms in all RAS isoforms. The GTP-bound conformation drives the cascade of signaling effects.

Based on these observations we have engineered the serine protease subtilisin to target the conserved QEEYSAM sequence in switch 2 of RAS (amino acids 61-67, **Fig. 1A**).

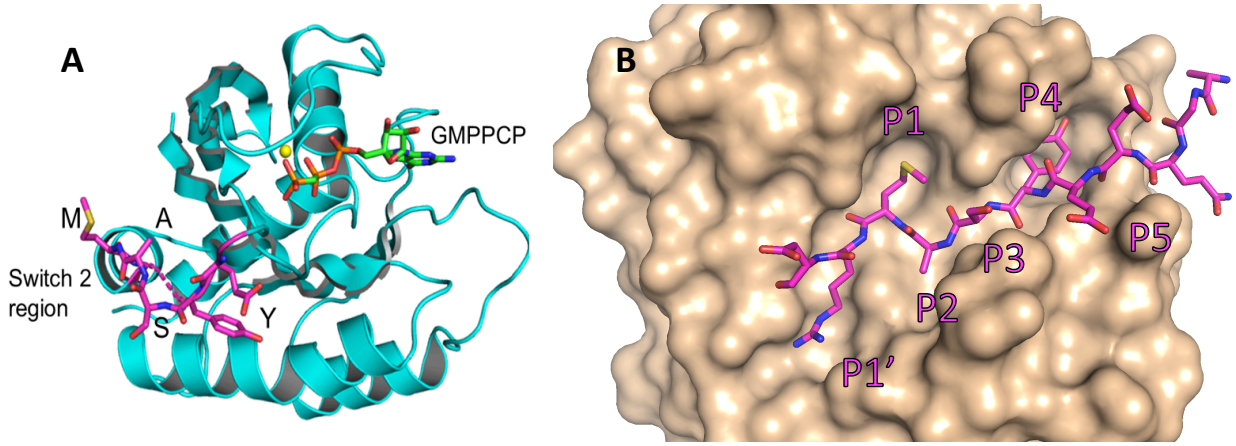

Fig. 1 A: Structure of RAS with a bound GTP analog (PDB code 6Q21), (4, 5), highlighting the YSAM site in Switch 2. B: RAS-specific protease based on an X-ray structure of 3BGO.pdb (6). Cognate sequence QEEYSAM-RD is modeled in the binding cleft. Substrate residues are denoted P1 through P5, numbering from the scissile bond toward the N-terminus of the substrate. Substrate amino acid on the leaving group side is denoted P1'.

Examination of several crystal structures of active RAS identified considerable conformational heterogeneity in switch 2 induced by a γ-phosphate on the nucleotide cofactor (4, 5, 7). We hypothesized that these structural changes would uncover a cryptic cleavage site, making the QEEYSAM target sequence more vulnerable to proteolysis in active RAS than in the inactive form. Motifs of this type generally occur in amphipathic helices because most of the amino acids have high α–helical propensity and also because the spacing between the large hydrophobic amino acids (Y and M) matches a helical periodicity.

Natural subtilisins have broad sequence specificity, but there is a wealth of information about engineering mutations that alter specificity (8-15). The major challenge to designing high-specificity proteases, however, is that specificity based on differential substrate binding falls far short of natural processing proteases. In many natural proteases the cognate sequence influences the chemical steps in peptide hydrolysis and not just binding steps (16). To engineer highly sequence-specific subtilisins we combined two previous observations: 1) Mutations at remote binding pockets for substrate side chains (sub-sites) can distort the subtilisin active site and (10, 12) 2) Mutating a catalytic amino acid in an enzyme can allow chemical rescue with a small molecule cofactor (6, 17). We leveraged these observations to create an engineered protease that requires both conformational and chemical rescue by the substrate and cofactor, respectively, in order to achieve high levels of activity. In particular, for the fully engineered RAS-specific proteases described here, binding of the cognate QEEYSAM sequence results in structural changes that are transmitted from the binding pockets to the active site and enable cofactor activation. In contrast, binding of non-cognate sequences adversely affects the active site and in fact antagonizes cofactor binding. These cofactor-dependent subtilisins strongly prefer dynamic regions of proteins (such as switch 2 in active RAS) over structured regions because efficient cleavage requires interactions with P5 to P1' amino acids in an extended conformation (**Fig. 1B**).

Engineered proteases were tested *in vitro*, in engineered *E. coli*, and in human cell culture. Major findings are the following: 1) Engineered proteases cut the QEEYSAM sequence in a synthetic peptide substrate with high specificity and are tightly-controlled by the cognate cofactor; 2) X-ray crystal structures of protease-substrate-cofactor complexes reveal interactions involved in substrate recognition and cofactor activation; 3) The QEEYSAM sequence in native RAS is cut in response to the cognate cofactor; 4) RAS-specific proteases cuts active (GTP) RAS 60-80 times faster than the inactive (GDP) form; 5) NMR analysis reveals that the QEEYSAM sequence is more dynamic in active RAS than the inactive form; 6) The level of RAS within *E. coli* cells can be regulated by co-expression of the RAS gene with different protease and cofactor combinations; 7) A RAS-specific protease can destroy RAS in mammalian cells.

RESULTS

Protease engineering The engineering process to develop specificity for the RAS sequence *QEEYSAM* involved extensive modification of the *Bacillus* protease, subtilisin BPN' (6, 17-24), a canonical serine protease in which the scissile peptide bond is attacked by a nucleophilic serine (S221). The nucleophilicity of S221 results from its interactions with the catalytic histidine (H64) and aspartic acid (D32) that together form a charge relay system (25). Most substrate contacts are with the first five amino acids on the acyl side of the scissile bond (denoted P1 through P5, numbering from the scissile bond toward the N-terminus of the substrate (26) and the first amino acid on the leaving group side (denoted P1', **Fig 1B**). Corresponding sub-sites on subtilisin are denoted S1', S1, S2, etc. Natural subtilisins have a strong preference for a hydrophobic amino acid at S1 and S4 sub-sites (**Fig. 1B**), but little discrimination for a particular hydrophobic amino acid (27, 28). The key to engineering high sequence-specificity was linking interactions in amino acid sub-sites to the rate of the first chemical step (acylation). In our design strategy, we considered two well-documented properties of proteases. The first is that certain mutations at sub-sites alter the conformation of remote catalytic residues (10, 12). The second observation

is that mutating a catalytic amino acid radically decreases activity of an enzyme (29, 30) but in certain cases allows some chemical rescue of activity by an exogenous small molecule that mimics the mutated amino acid (31-33). **The design strategy was based on the hypothesis that a linkage between substrate binding and chemical rescue can be created by mutating sub-sites to optimize interactions with the desired cognate sequence and combining these with mutation of a catalytic amino acid.** To test the robustness of this hypothesis we generated two different active site variations: 1) D32G variants that are activated by nitrite or azide; 2) H64G variants that are activated by imidazole (6, 17). Initial design was based on the X-ray structure of an inactive (D32A, S221A) variant of subtilisin (3BGO.pdb) (6). The structure shows the enzyme bound to a cognate peptide (LYRAL-SA) and azide in the position normally occupied by the catalytic D32. The substrate binding pockets and the azide binding site form an interconnected network (**Fig. S1**) (9, 12, 34, 35). The theory is that binding at one sub-site can influence interactions in other parts of the network. The desired cognate sequence QEEYSAM-RD for RAS was modeled into the binding cleft of the 3BGO.pdb structure. Amino acid substitutions were introduced into the model and protein-protein and protein solvent interactions were evaluated by visual inspection (36). Based on this analysis, as well as earlier engineering work, we designed mutations in the catalytic region, the S1 pocket, and the S4 pocket to create a nitrite-dependent (D32G) protease and an imidazole-dependent (H64G) protease (TABLE 1). These are denoted Protease1(N) and Protease1(I), respectively. These mutants were expressed, purified, and characterized for activity and specificity using substrate series that was originally used to characterize the progenitor protease: sDXKAM-AMC, where X = Y, F, I, or L (6, 17, 22, 24). AMC is the fluorogenic leaving group, 7-amino-4-methylcoumarin. Activity of both proteases is highest for P4 = F with lower activity for P4 = Y, I, and L (**Fig. S2**). The X-ray crystal structure of Protease1(N) was determined in complex with a cognate peptide LFRAL. We used the Protease1(N) structure to model additional mutations to increase specificity for P4 = Y.

TABLE 1: Engineering progression and mutations in the catalytic, S1, and S4 regions

Protease*/position	30	32	33	62	64	68	101	104	107	128	135	166
subtilisin BPN'	V	D	S	N	H	V	S	Y	I	G	L	G
Protease1(N)	I	G	T	S	H	I	S	A	V	S	L	T
Protease1(I)	I	D	T	S	G	I	S	A	V	S	L	T
Protease2(N)	I	G	T	S	H	I	S	A	I	S	V	T
Protease2(I)	I	D	T	S	G	I	S	A	I	S	V	T
RASProtease(N)	I	G	T	S	H	I	K	A	I	S	V	T
RASProtease(I)	I	D	T	S	G	I	K	A	I	S	V	T

*Engineered proteases have mutations at 18 positions in addition to those specified above (6).

On the basis of this analysis we introduced V107I and L135V mutations in the S4 pocket. This created the second pair of mutants: Protease2(N) and Protease2(I) (**Table 1**). These variants exhibited considerable preference for the substrate sDYKAM-AMC. Thus, when P4 is F instead of Y, k_{cat}/K_M falls by more than two-fold. All other variations at P4 result in a greater than 50-fold decrease in k_{cat}/K_M. Protease2(N) and Protease2(I) were further evaluated with peptide-AMC substrates with variations at P1, P2, and P4. Both proteases show high preference for P4 = Y or F, P1 = M or L, and a moderate preference for P2 = A. Data for Protease2(I) are shown in **Fig. 2**.

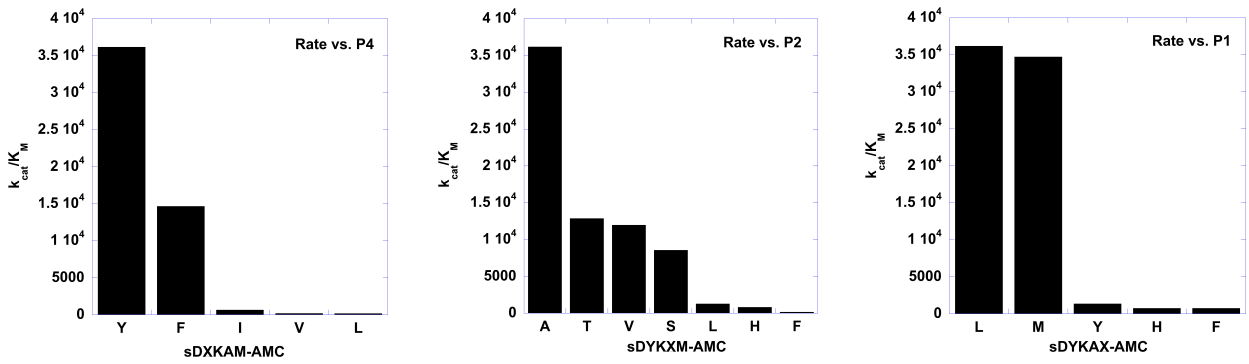

Fig. 2: *Evaluating specificities in the process of engineering a RAS-specific protease.* Protease2(I) evaluated with peptide-AMC substrates with variations at P4, P2, and P1.

Finally, we examined variations to increase activity for P3= S and P5= E. Protease mutants at 101 (S, K, R) and 103 (Q, R) were evaluated using the peptide substrates QEXYSAM-AMC, where X = E, R, I, or L and QEEYXAM-AMC, where X = S, R, or E. The S101K mutants gave a high preference for the desired cognate sequence QEEYSAM. The

S101K mutants were further analyzed for activity using the peptide substrate QEE**Y**SAM-AMC. **Fig. S3** compares k_{cat}/K_M as a function of nitrite concentration for Protease2(N) and the S101K mutant. The figure shows that the S101K mutation increases k_{cat}/K_M by six fold in 1mM nitrite. The two S101K mutants are denoted as RAS-specific proteases RASProtease(N) and RASProtease (I).

Synergy between conformational and chemical rescue Comparing nitrite activation in RASProtease(N)with the cognate substrate (QEE**Y**SAM-AMC) versus a near cognate (QEE**I**SAM-AMC) revealed a linkage between cognate substrate binding and co-factor activation (**Fig. 3A**). In 1mM nitrite k_{cat}/K_M is ~ 100-fold greater for P4 = Y versus I. The low activity of RASProtease(N) with the near cognate substrate is partly because of weaker substrate binding (5.5-fold less for P4 = I than P4 = Y) but mostly because of a lack of cofactor activation when P4 = I. A similar phenomenon is observed with RASProtease(I). The k_{cat}/K_M value is ~300-fold higher for the cognate P4=Y versus P4 = I in 1mM imidazole (**Fig. 3B)**.

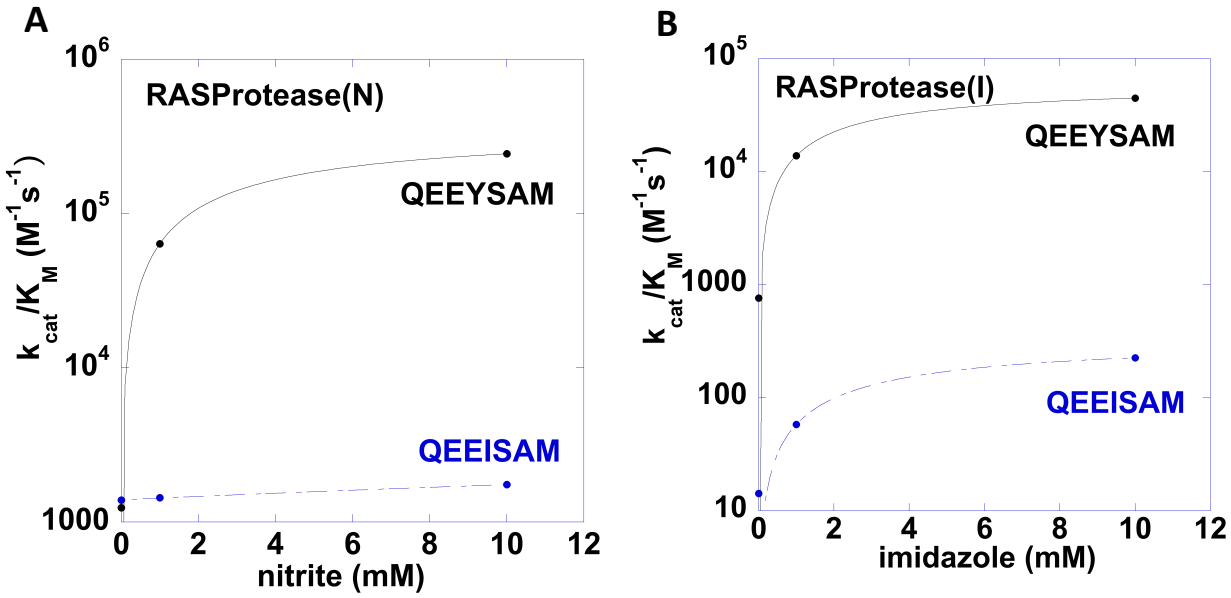

Fig. 3 *Conformational and chemical rescue by native and near-native sequences* **(A)** k_{cat}/K_M as a function of nitrite concentration for RASProtease(N) with the substrates QEEYSAM-AMC and QEEISAM-AMC: (**B**) k_{cat}/K_M as a function of imidazole concentration for RASProtease(I) with the substrates QEEYSAM-AMC and QEEISAM-AMC.

Structural Analysis of Protease Interactions with the Switch 2 Target Sequence To understand the structural basis for specificity and cofactor activation, we determined crystal structures of RASProtease(I) alone, in complex with YSAM and QEEYSAM product peptides, and with imidazole (**Fig 4, S4**). We compared these structures with the crystal structure of Protease1(N) in complex with a peptide corresponding to its sequence specificity (LFRAL, **Fig. 4B**).

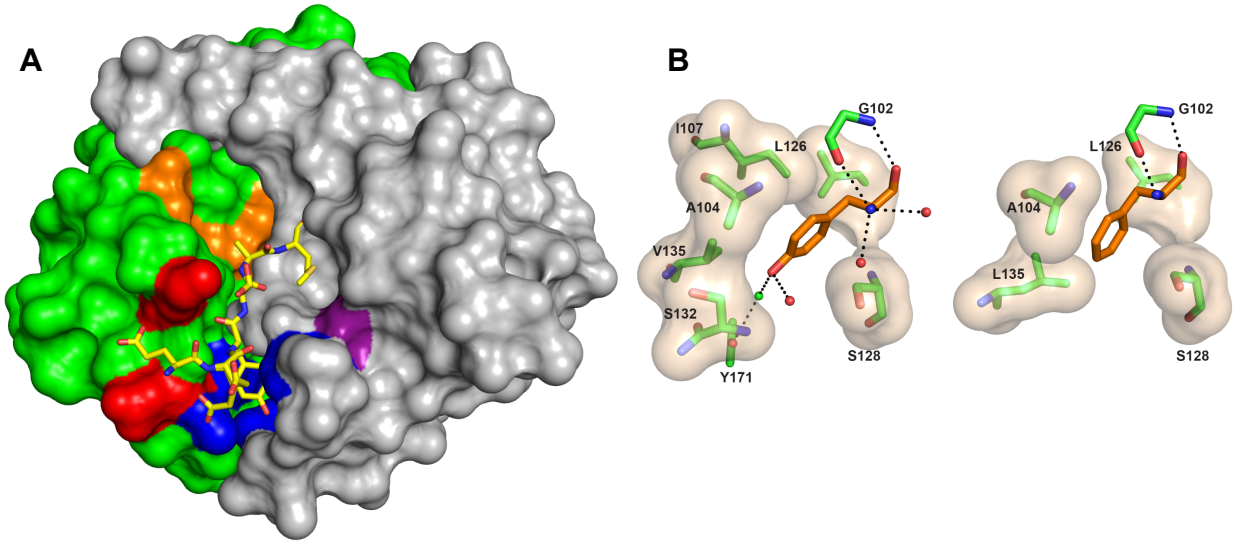

Fig. 4: *Engineering a protease directed against active RAS* (**A**) Surface representation of RASProtease(I) with substrate binding sites colored purple (S1), orange (S2 and catalytic residues), red (S3), and blue (S4) with the bound YSAM peptide overlaid. (**B**) Interactions at the P4 site of RASProtease(I) (left) and its progenitor Protease1(N) (right). The van der Waals interactions between residues in the protease active site (carbons colored green) and the bound P4 residue (carbons colored orange) are represented as a tan surface. Hydrogen bonds are represented as black dashed lines.

Overall the structures are very similar, with an RMSD between Cα carbons of 0.17 Å. The aromatic ring of the P4 side chain has common van der Waals interactions: the Cα and Cβ atoms of A104 interact with Cε1, the Cδ1 of L126 interacts with Cδ2, and Cβ of S128 interacts with Cδ2 and Cε2. Because of the space created in the S4 pocket by the L135V mutation, either a water or an ion coordinates the hydroxyl of P4 Tyr, the hydroxyl of Y171, and the backbone nitrogen of S132 in RASProtease(I) (**Fig. 4B, Fig. S4**). We currently have this modeled as a chloride ion based on the peak height observed in an anomalous difference fourier map;

however, added chloride does not appear to influence kinetic properties. P4 interactions are facilitated by a significant shift of the loop containing residues 130 to 133 of RASProtease(I) relative to the Protease1(N) complex. In fact, these are the only residues in the entire structure whose Cα positions shift by more than 1 Å, including the N- and C-termini. This structural remodeling reflects what we intended (i.e. creating a stable state that only exists when substrate is bound) but the mode of conformational rescue is not what we expected.

In contrast to P4, the changes to the P3 site are more limited (**Fig S5**). Mutation of S101K increases activity with Ser at the P3 position. Hydrogen bonding interactions between the backbone nitrogen and carbonyl oxygen of the P3 residue and the corresponding partners on residue G127 are conserved.

The structures also provide insight into the structural basis for cofactor activation by both nitrite in Protease1(N) and imidazole in RASProtease(I). In both cases a catalytic amino acid is mutated to Gly and the vacated space is occupied by a network of conserved water molecules in the absence of the cognate cofactor. Nitrite was modeled into the solvent network of the Protease1(N) structure (replacing HOH 54; **Fig. S6A**) such that it supplies the critical H-bond to the catalytic H64 and is coordinated to N33 and three conserved waters (23, 302, and 382). The coordination sphere of nitrite in Protease1(N) appears to be more complete than observed for azide in the parent enzyme (3BGO) and suggests why nitrite is tightly bound in spite of its lower pKa (3.37, compared to 4.72 for azide). Structures of RASProtease(I) without imidazole have three conserved waters (19, 81, and 122) that interact with Oδ1 and Oδ2 of D32, CO of S125, NH of G64, Oγ of S62, and Oγ of S221. When imidazole binds, these waters are displaced, the imidazole nitrogens H-bond to Oδ1 and Oδ2 of D32 and Oγ of S221, and the charge relay system is reconstituted (**Fig. S7, S6B**). An additional Interesting feature of the structure of RASProtease(I) with QEEYSAM was the presence of an acyl adduct between the C-terminus of the P1 Met of the peptide and the Oγ of S221 of the enzyme (**Fig S4**). Apparently

the binding energy of the QEEYSAM peptide is sufficient to push its terminal carbon and Oγ of S221 into an orientation that drives the equilibrium from a product complex to the acyl enzyme (37). Studying these types of subtle changes to the water structure in the active site that occur upon substrate and cofactor binding will allow us to make further changes to promote chemical and conformational rescue.

Cleavage of RAS(GDP) and RAS(GMPPNP) The next step in assessing our RAS-specific proteases was to monitor cleavage of the intact protein, wherein switch 2 would adopt a range of conformations from extended to helical. Moreover, measuring protein cleavage allowed us to assess the relative rates of cleavage for active versus inactive RAS, thereby testing our hypothesis that active RAS is more vulnerable to proteolytic attack due to increased dynamic motion in switch 2.

a) Gel assays: We next determined the specificity of RAS proteases for active RAS. To trap RAS in an active conformation, we used an adduct with guanosine 5′-[β,γ-imido]triphosphate (GMPPNP), a slow hydrolyzing analog of GTP. **Fig. 5A** shows the kinetics of digestion of 1μM RAS(GDP) and RAS(GMPPNP) with 1nM RASProtease(N) in 1mM nitrite. Reactions of RAS(GDP) and RAS(GMPPNP) with RASProtease(I) were also compared (data not shown). In summary, RAS(GMPPNP) cleavage is always faster than that observed for RAS(GDP) but detailed kinetic analysis is difficult because of limitations in quantitation of bands on a gel. Analysis by MALDI confirms that the enzyme cleaves RAS after the QEEYSAM site with no off-target cleavages (**Fig. S8**). No cleavage of RAS is observed in the absence of a cognate cofactor.

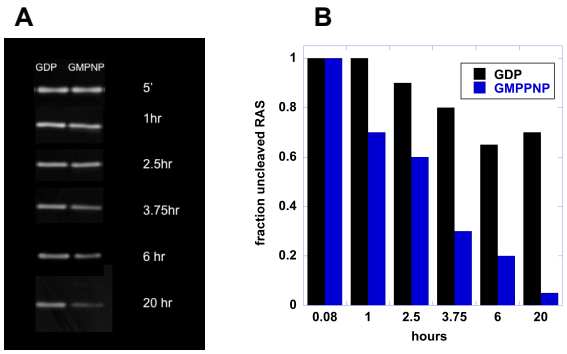

Fig. 5: *Analysis of RAS cleavage* **(A)** The timing of RAS cleavage by 1 nM RASProtease(N) in 1 mM nitrite. At each time point (top to bottom), the 19,315 dalton RAS band from an SDS gel is shown for the RAS(GDP) and RAS(GMPNP) digests; (**B**) Normalized band density ± 10% (three replicates).

b) Quantitative assays of RAS interactions with protease: We further analyzed the RAS cleavage reaction to achieve a quantitative understanding of individual steps in the reaction pathway. A minimum realistic mechanism is as follows:

$$\mathbf{R + P} \overset{K_S}{\rightleftharpoons} \mathbf{RP} \overset{k_2}{\rightharpoonup} \mathbf{Pr_1 + r_2} \overset{K_P}{\rightleftharpoons} \mathbf{P + r_1 + r_2} \qquad \textbf{mechanism 1}$$

Where R = RAS, P = protease, r_1= the RAS N-terminal cleavage product and r_2= the RAS C-terminal cleavage product. K_S is the dissociation constant for uncleaved RAS and k_2 is the rate of the first chemical step in peptide bond cleavage (acylation). K_P is the dissociation constant for the r_1 product fragment. To accurately determine kinetic parameters for RAS cleavage, we measured the kinetics of QEEYSAM-AMC cleavage in the presence of RAS(GDP), RAS(GMPPNP). Data for RASProtease(I) are shown in **Fig. 6A and B**. The concentration of RAS(GMPPNP) or RAS(GDP) was varied from 0 to 20μM. Interaction of protease with RAS is manifested as inhibition of peptide-AMC cleavage by RAS and RAS cleavage products. Early in the progress curves, the major inhibitory species is native RAS. As the reaction progresses, inhibition increases as the concentration of the r_1 fragment increases. K_P of r_1 was determined in an independent series of experiments. To accomplish this, a fragment corresponding to the N-terminal cleavage product of RAS (amino acids 1-67, ending at YSAM) was expressed in *E. coli* and purified. Inhibition of protease by r_1 was measured by varying its concentration from 50nM

to 3.3μM in reactions of each protease and with 0.1, 0.5, and 1μM QEEYSAM-AMC (**Table 2**). NMR analysis of cleaved RAS shows that both r_1 and r_2 are disordered (**Fig. S9**). Independent measurements of binding uncleaved RAS with protease were made by gel filtration in the absence of cofactor (**Fig. S10**). Kintek Explorer was used to fit all data to mechanism 1 (**Fig. 6, Table 2**). Values of k_2/K_S were calculated to compare specificity for active RAS, independent of the r_1 product dissociation rate (**Table 2**). The analysis shows that k_2/K_S for RASProtease(I) in 1mM imidazole is ~60 times faster for RAS(GMPPNP) compared to RAS(GDP). Similar measurements and global fits also were made for RASProtease(N) in 1mM nitrite (**Fig. S13**) with similar specificity (80-fold) for RAS(GMPPNP).

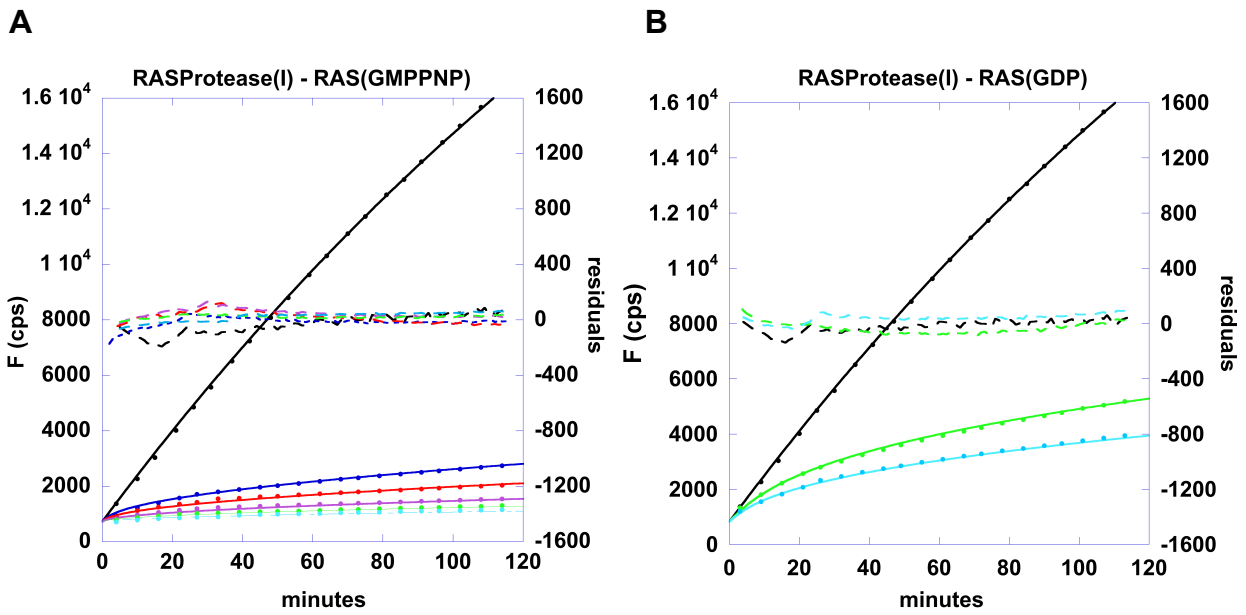

Fig. 6: *Kinetics of AMC release from QEEYSAM-AMC by 100nM* RASProtease(I) *in the presence of RAS* (**A)** RAS(GMPPNP); (**B)** RAS(GDP). The concentration of RAS was 0 μM (black), 1 μM (blue), 2 μM (red), 5 μM (violet), 10 μM (green), and 20 μM (cyan) in the presence of 1 μM QEEYSAM-AMC and 1 mM imidazole. Data points are solid circles. Global fit to mechanism 1 are solid lines. Residuals of data minus fits (5x scale) are dashed lines.

Table 2: Kinetic parameters for RAS(GMPPNP) and RAS(GDP) cleavage using global fitting.

Protease	cofactor	k_2 / K_S	K_P
RASProtease(I)/RAS(GDP)	1mM imidazole	220 $M^{-1}s^{-1}$	30nM
RASProtease(I)/RAS(GMPPNP)	1mM imidazole	13,720 $M^{-1}s^{-1}$	30nM
RASProtease(N)/RAS(GDP)	1mM nitrite	410 $M^{-1}s^{-1}$	40nM
RASProtease(N)/RAS(GMPPNP)	1mM nitrite	32,430 $M^{-1}s^{-1}$	40nM

K_P is ± 5%.

Analysis of the target region in RAS by NMR To better understand how dynamics in switch 2 contribute to RAS protease specificity for the active form, we examined the dynamics of this region by NMR. An order-to-disorder transition of switch 2 has been previously observed in RAS crystal structures (38, 39). Two-dimensional ^{1}H-^{15}N HSQC spectra indicate extensive structural differences between the GDP- and GMPPNP-bound forms of RAS (**Fig. S11A,B**). NMR backbone resonance assignments were made using standard procedures and deposited in BioMagResBank (accession codes for the GDP and GMPPNP forms are 28008 and 28009, respectively). Most of the amide signals in the switch 1 (residues 30-38) and switch 2 (residues 59-76) regions are detectable in the GDP-bound state but are exchange broadened in the GMPPNP-bound form, indicating enhanced dynamics in the GMPPNP state on the NMR timescale (microseconds to milliseconds). Comparable observations have been made with WT HRAS, WT KRAS, and other RAS mutants (40-47). Analysis of differences in backbone dynamics using ^{15}N-relaxation measurements indicates that the GMPPNP-bound form of RAS is also considerably more flexible on the ps-ns timescale than the GDP-bound form (**Fig. S11C, Fig. S12**). Thus, the effect of GMPPNP binding is to increase main chain flexibility for a large number of residues in the molecule over a wide timescale range, making the GMPPNP- and GTP-bound states, and the switch regions in particular, more susceptible to proteolytic cleavage than the GDP-bound form.

Co-expression of RAS with RASProtease(I) ***in E. coli*** To measure activity and specificity in cells, we developed a bacterial system for co-expressing RAS with RAS-specific proteases. We constructed genes for RAS fusion proteins (**Fig. S14**) that consisted of an N-terminal G_A domain (48, 49), amino acids 1-166 of human RAS, and a C-terminal cellulose binding domain (50). The small N-terminal and C-terminal binding domains allow easy purification of the entire fusion protein as well as both cleavage products so that the precise cleavage site in *E. coli* can be determined. The expression of the RAS fusion protein is shown in **Fig. S15**. Proteases from genes for the zymogens were co-expressed with the RAS fusion proteins. The protease zymogen (34.9kDa) consists of an N-terminal inhibitory (I) domain (8.5kDa) and the protease domain (26.4kDa) (51). Growth was at 37˚C with 100μM imidazole added to the culture medium (**Fig. 7**). **Fig. S16** shows a control expression time course without imidazole. The gel patterns show that RAS cleavage is dependent on imidazole and coupled to the degradation of inhibitory domain of the protease zymogen, with RAS fragments r_1 and r_2 appearing as intact inhibitor decreases. By 41 hrs. in imidazole, all inhibitor is cleaved and greater than 50% of RAS is cleaved (**Fig. 7**). The gel pattern also shows that RAS is specifically cleaved into two discrete fragments. We confirmed that RAS was cleaved after the QEEYSAM sequence by purifying the r_1 fragment from the *E. coli* extract and measuring its mass by MALDI. There is no indication in the gel pattern of *E. coli* proteins being degraded. The fact that ~50% of RAS remains intact after 41 hrs is consistent with a high RAS protease preference for active RAS in the cell. Newly synthesized RAS predominantly binds GTP and therefore initially exists in the dynamic, active conformation. RAS(GTP) then converts to RAS(GDP) at a rate of ~1 hr^{-1} (52-54). Because *E. coli* lacks GDP-GTP exchange factors, we assume that RAS remains in the GDP bound form after hydrolysis and is less vulnerable to cleavage. After new

RAS synthesis stops, RAS accumulates in the inactive and partially protease-resistant form.

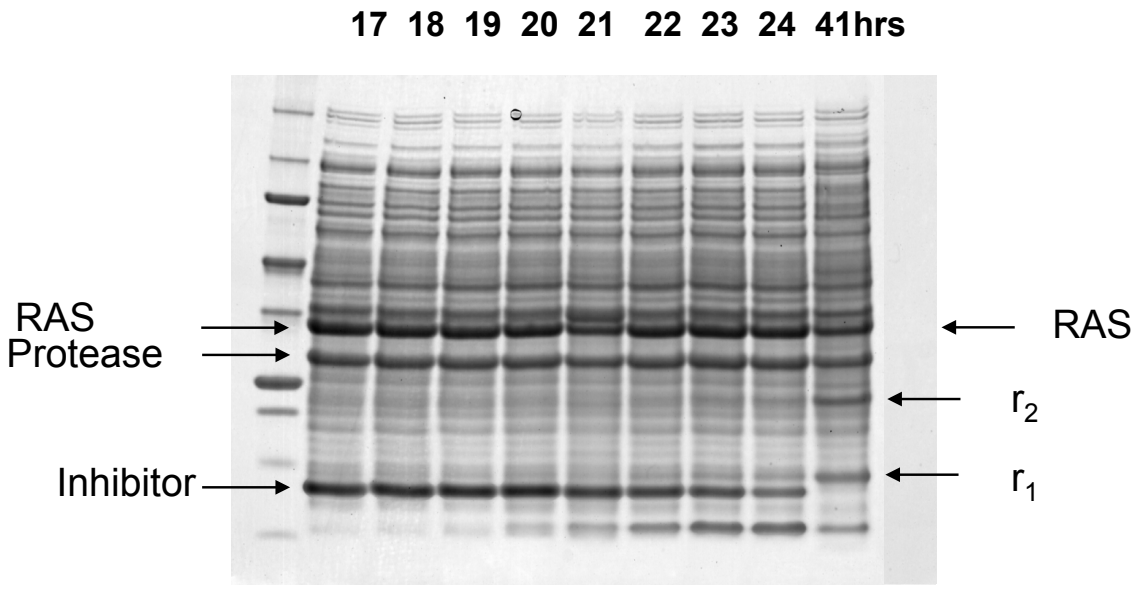

Fig 7: RASProtease(I) with 100μM imidazole added to the culture media at 17hrs. Intact RAS fusion protein is 35,974 daltons. The N- and C- terminal fragments are 13,579 (r1) and 22,413 daltons (r2), respectively. Markers: 250, 150, 100, 75, 50, 37, 25, 20, 15, 10 kDa.

Co-expression of RAS with RASProtease(N) **Fig. S17** shows co-expression of the RAS gene with the RASProtease(N) zymogen gene. RASProtease(N) cleaves ~ 70% of RAS into two discrete fragments within 18hrs of growth but the remaining RAS remains intact after 48 hrs. Unlike the case with imidazole, we are not able to precisely control nitrite concentration because it is an intermediate in metabolic pathways involving nitrogen in *E. coli* (55, 56). Nevertheless, the RAS cleavage by nitrite-activated proteases is potentially informative because nitrite is a disease marker in eukaryotic cells and its concentration in *E. coli* is likely similar to that in cancer cells (55, 56). RASProtease(N) appears to be more active in *E. coli* with endogenous nitrite than RASProtease(I) in 100μM imidazole. Even so, a cleavage-resistant population of RAS remains after 48 hrs. We presume this is RAS(GDP).

Engineered proteases can destroy active RAS in mammalian cells FInally, we tested whether a protease RASProtease(N) could cleave the switch 2 target sequence in a human cell. Based on our NMR data and fact that switch 2 is conserved among the 3 major

RAS isoforms, any RAS isoform would be appropriate for this type of experiment. However, since KRAS is the most important cellular and therapeutic target, we used KRAS as our target for cell-based experiments. We employed fluorescently-tagged RAS (eGFP-KRAS) as a means to simplify detection of cleaved product. This fusion (48 kDa) can be observed in a Western blot probed with an anti-GFP monoclonal antibody (Abcam, **Fig. 8A**, lane 1). Induction of expression of the pro-protease with doxycycline results in a marked depletion of eGFP-RAS and a corresponding increase in the presence of a band consistent with the eGFP protein from the fusion (**Fig. 8A**, lane 2). This change in migration does not occur with an inactive mutant of RASProtease(N) (S221A) with or without doxycycline (**Fig. 8A**, lanes 3 and 4). Probing the same samples with an anti-RAS antibody (Ras10, ThermoFisher) confirms that this band contains an eGFP-RAS fusion and further shows that RAS disappearance coincides with the appearance of the eGFP product (**Fig. 9A**, lanes 1 vs. 2). As expected, primary processing of the RASProtease(N) zymogen (34.9kDa) to the mature protease (26.4 kDa) occurs readily in cells (**Fig. 8A**, lane 2). Primary processing is not observed for the S221A mutant (i.e., compare **Fig. 8A**, lanes 2 and 4). In addition, fluorescence microscopy images show a marked decrease in eGFP signal upon induction of the active protease but not the inactive protease (**Fig. 8B**). Disappearance of the eGFP-RAS fragment indicated that, as in *E. coli*, cleaved RAS is further degraded by cellular proteases.

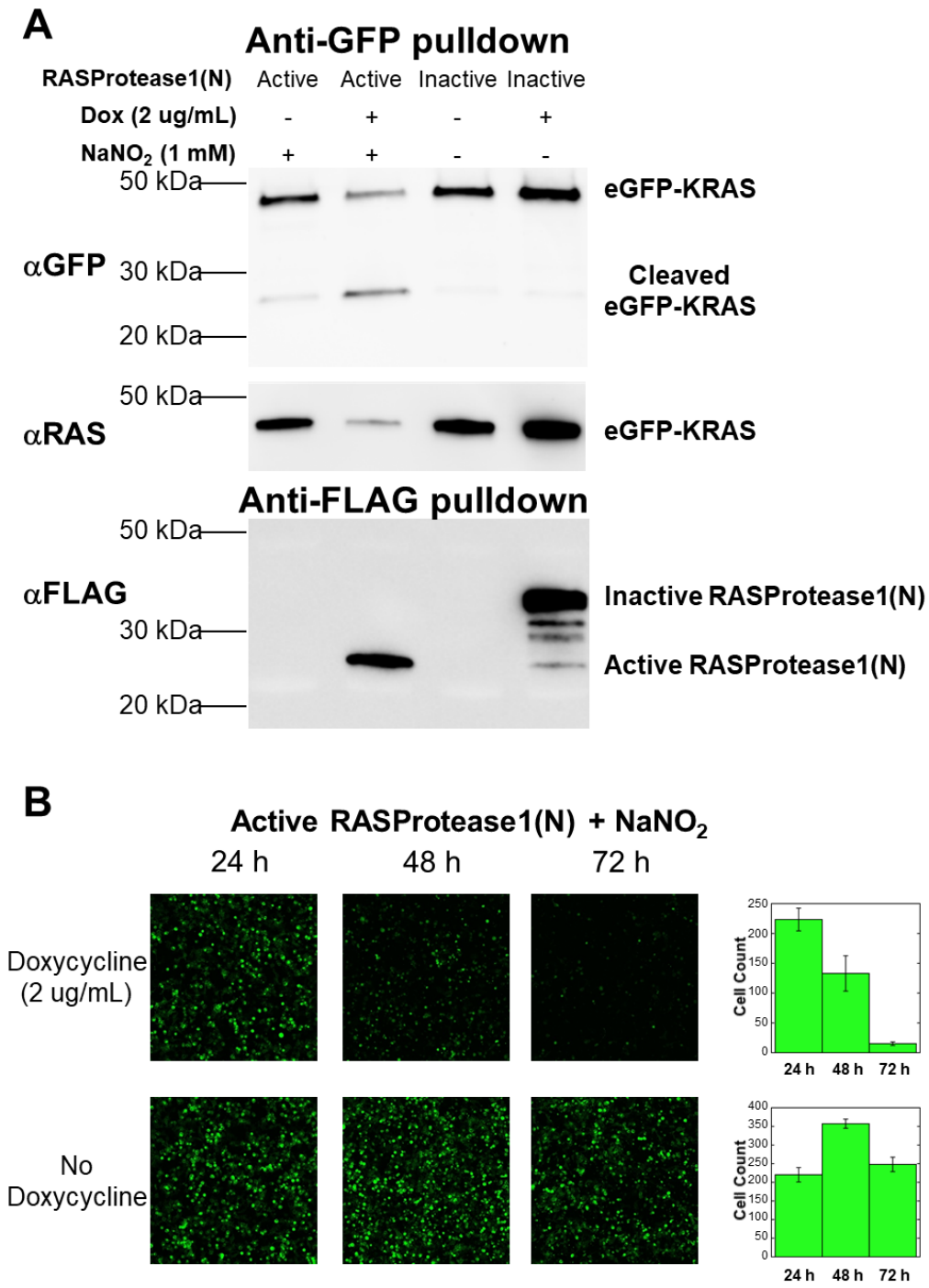

Figure 8: *RAS-specific protease activity in cells* (**A**) Western blot analysis of cells co-transfected with eGFP-RAS and either active or inactive (S221A) RASProtease(N) shows the appearance of a RAS cleavage product upon induction of the active protease when probed with an anti-GFP antibody following a GFP pull-down. Appearance of this product coincides with depletion of a RAS-reactive band when probed with an anti-RAS antibody. Appearance of cleaved eGFP-KRAS also coincides with expression of activated protease that has cleaved its inhibitory I-domain, but not with inactive pro-protease. (**B**) Induction of the active protease in HEK 293T cells at 24 hours after transfection with nitrite-supplemented culture medium results in a marked decrease in GFP fluorescence at 48 and 72 hours after transfection compared to the same cells without induction of protease expression.

DISCUSSION

Our goal in this work was to develop principles for engineering protein-specific proteases and to apply these principles to target active RAS. The key to engineering high sequence specificity in a protease is linking binding at sub-sites with chemical steps in peptide bond hydrolysis. This was accomplished by exploiting two facts about enzymes: 1) Mutations at remote sub-sites can affect the conformation of catalytic amino acids; 2) Change in the conformation of the catalytic region affects chemical rescue of active site mutants. High-specificity occurs when cognate sequence binding at sub-sites is compatible with productive binding of cofactor but binding of incorrect sequences antagonizes cofactor binding.

Engineering specificity using substrate and chemical rescue To understand the engineering process, it is useful to consider some basic structural features of subtilisin proteases. Subtilisin has a cardioid shape with the active site and substrate binding pockets forming a cusp that divides N-terminal and C-terminal domains (**Fig. 9**, (28)).

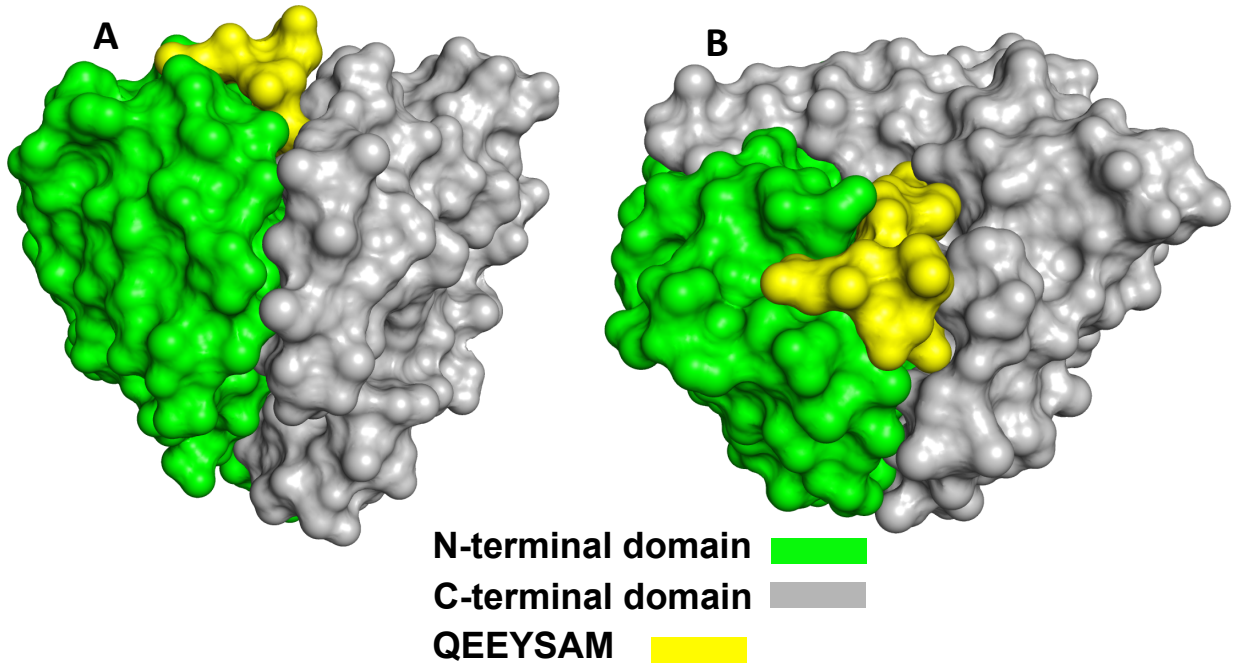

Fig. 9: Two views of the domain structure for subtilisin (6UAO.pdb) with substrate bound .

The catalytic D32 and H64 and the P2, P3, and P5 sub-sites are primarily associated with the N-terminal domain (**Fig. 4A**). The catalytic S221 and P1, P4 and P6 sub-sites are primarily associated with the C-terminal domain. Thus the substrate intercalates between the two domains, bridges the interface, and affects the association between the two. Subtilisin specificity in general can be understood in terms of a model in which the domain interface is either in a deformed, low-activity conformation or in a canonical active conformation. When the domain interface is stable, the substrate adapts to the enzyme and specificity is broad. This has also clearly been shown for α–lytic protease which resists deformation of catalytic amino acids even as binding pockets conform to bind a range of substrate sequences (57). When the stability of the domain interface of a protease is decreased by mutation, however, the enzyme conforms to the substrate and activity will be low unless the substrate fit is precise and promotes the active conformation (i.e. in part by reestablishing the native interface between domains). Because individual sub-sites and the catalytic triad are interconnected, distortion in one area affects the other. Rheinnecker *et al*. (10, 12) have shown previously that certain mutations in the S4 pocket of subtilisin, particularly those that form cavities, adversely affect activity of even small substrates that do not interact at S4. This led to an increase in specificity for peptide substrates with L or F over A at P4. To create RAS-specific proteases, we combined traditional sub-site engineering approaches with mutations that destabilize the domain interface. The best mutations weaken the interface between the two domains but generate favorable interactions with a cognate substrate and/or the cofactor. The favorable interactions rescue the active site conformation at the interface resulting in high activity. For example, removing a catalytic residue (e.g. D32G or H64G*)* reduces activity both by eliminating an element of the charge relay system and weakening the domain interface, but also creates potential for rescuing the active conformation and chemistry by the cognate cofactor and substrate. Likewise, enlarging the S4 pocket to accommodate tyrosine causes instability that is transmitted to the weakened catalytic site. Binding of the cognate substrate with a P4 tyrosine rescues the active

conformation, however, by supplying stabilizing interactions in the S4 pocket that are transmitted to the catalytic region and promote productive binding of cofactor. The magnitude of cofactor activation depends on the population of the active conformation in the apo enzyme relative to its population with substrate and co-factor bound. This is a delicate balance. If the domain interface is too stable, a mutant will be fast but non-specific. If the interface is too unstable, however, a mutant will be specific but slow. To produce high specificity and activity, the energies of the inactive and active conformations must be close enough that cognate binding to sub-sites significantly populates the active form (58). This creates a critical state in which both cofactor binding and cognate sub-site interactions become required for activity. These proteases have very low activity against all substrates in the absence of cofactor, but allow rescue of the active conformation by the cognate sequence with its cofactor.

Comparing several high-resolution structures reveals structural changes that may contribute to the ability of cognate substrate and cofactor binding to rescue activity in RAS-specific proteases. RAS-specific proteases have an expanded S4 site that binds numerous solvent molecules in the enlarged S4 pocket. Structures with a cognate peptide bound show that the L135V mutation allows space for an adventitious ion-binding site that coordinates the hydroxyl group of the P4 tyrosine of the substrate. This stabilizing interaction may be an important element for rescuing the active conformation of the catalytic region and enabling strong cofactor activation. Likewise, mutating a catalytic amino acid to Gly creates space that is occupied by a network of conserved waters in the absence of the cognate cofactor.

It might be assumed that enzymes engineered in this way would be slow (59). This is not true. Kinetic analysis shows proteases targeting RAS are both more specific and more active than the viral processing proteases TEV and HRV 3C are for their cognate sequences (60, 61). For example, in the presence of 1mM cofactor, RASProtease(N) and RASProtease(I) have k_{cat}/K_M of > 10^4 $M^{-1}s^{-1}$ compared to k_{cat}/K_M values of ~10^3 $M^{-1}s^{-1}$ for 3C-type proteases.

Engineering cofactor activation also proved to be useful for regulating protease activity inside cells. Imidazole is benign but normally not present inside cells. Thus it can be used as a xenobiotic activator to tightly control RAS cleavage in *E. coli*. Controlling RAS cleavage in *E. coli* with nitrite is more complicated because it is an intermediate in metabolic pathways involving nitrogen. Nitrite may be quite useful for regulating activity in eukaryotic cells, however. Elevated nitrite is a common signature of disease states (including RAS-related cancers) (62-64) and reaches concentrations >100μM in tumor cells (65, 66). This occurs because disease-induced nitric oxide synthase produces nitric oxide (NO) and NO quickly oxidizes and accumulates as nitrite.

Using the conformation of the target protein to increase specificity. Primary structure alone is generally insufficient for encoding protease specificity. For example, Caspases are considered highly specific, but it is not possible to predict their natural protein targets from their cleavage patterns on small peptides (67, 68). Thus, a critical element of specificity is discrimination between different conformations of the same sequence. To do this, we chose a target sequence that is partially exposed in active RAS but is typically found in amphipathic α-helices and resistant to proteolysis when it occurs in other proteins. NMR analysis indicated extensive structural changes between the GDP- and GMPPNP-bound forms of RAS and increased mobility of the QEEYSAM sequence in RAS(GMPPNP). Specificity is governed therefore by both the correct primary structure and dynamic changes in the secondary structure of the target region. The additional information from conformation allows much higher specificity than can be achieved based on sequence alone. The effectiveness of this type of recognition is manifested in the 60 to 80-fold difference in cleavage rate between active and inactive RAS. In this sense inactive RAS serves as an internal control. To be useful in a cell, a protein-specific protease must selectively destroy the target protein and not many competing substrates. Experiments with RAS-specific proteases in cells show this to be the case.

Significant depletion of RAS can be achieved without any apparent effect on cell viability or noticeable degradation of endogenous proteins.

In conclusion, the principles presented here are general and can be applied to many target proteins. This includes proteins involved in aberrant signal transduction but also includes foreign proteins involved in cell invasion. The process of creating new protein-specific proteases begins with matching the specificity of an existing protease with changes in local or global stability in a desired target protein. It ends with designing-evolving the protease to match the new target sequence and cofactor environment.

MATERIALS AND METHODS

Mutant subtilisins Expression and purification was performed as essentially described (69, 70).

Kinetic measurements Initial characterization of different protease-inhibitor combinations was carried out using a KinTek Stopped-Flow Model SF2001. Kinetic measurements of longer reactions, after manual mixing, were determined using a BioTek Synergy HT plate reader.

Protein Expression and purification of RAS The genes for human HRAS (amino acids 1-166) were cloned into the vector pPal8 (17), which encodes an engineered subtilisin pro-sequence as an N-terminal fusion domain. The resulting fusion proteins were produced in *E. coli* and purified using an affinity-cleavage tag system, which we developed (17), essentially as described in (71). A commercial version of the purification system is available through Bio-Rad Laboratories (Profinity eXact Purification System). Exchange of GDP in recombinant preps (72) for GMPPNP was performed as described in (73).

Cell lines and plasmid constructs HEK 293T cells (74) were purchased from ATCC. ORFs for protease clones were synthesized by Genscript (Piscataway, NJ) and subcloned into pLVX-TetOne-Puro. The eGFP-KRAS plasmid was provided by the RAS Initiative (Frederick, MD).

NMR spectroscopy NMR spectra of RAS-GDP and RAS-GMPPNP were recorded on a Bruker Avance III 600 MHz spectrometer fitted with a cryoprobe.

Crystallization, data collection and processing Purified RASProtease(I) was concentrated to 7 mg/mL for use in crystallization screening. The best crystals from our screens were obtained in a condition containing 0.1 M Bis-TRIS propane pH 8.5, 0.2 M KSCN, and 20% PEG 3350. Crystals appeared overnight and grew to a maximum size after 2-3 days. These crystals belong to space group $P4_12_12$ and have unit cell dimensions a=b=58.6 Å, c=124.8 Å, $\alpha=\beta=\gamma=90°$. Native data up to 1.7 Å resolution were collected using in-house X-ray diffraction resources.

Analysis of RAS cleavage in cells HEK 293T cells were seeded into 6-well plates at a density of 1.2 x 10^6 cells per well in DMEM plus 10% Tetracycline-free FBS. Sixteen hours after seeding, cells were transfected with 1.25 µg of each plasmid using Lipofectamine 3000 (Thermo Fisher) according to the manufacturer's protocol. Transfected cells were incubated for 24 hr at 37 °C in a humidified incubator providing 5% CO_2. Twenty-four hours after transfection, expression of the protease was induced by addition of doxycycline to fresh media at a final concentration of 2 µg/mL, followed by incubation at 37 °C for an additional 48 hr.

Additional details of all methods are given in Supplemental information.

Acknowledgements

The authors thank Vanessa Wall, Dominic Esposito, and Frank McCormick (NCI-Frederick) for scientific guidance and reagents, including the eGFP-KRAS reporter plasmid. Dominic Esposito also critically read the manuscript and gave helpful suggestions. This work was supported by MPower-IBBR (University of Maryland) Seed Funds, R44CA163403 (Ruan and Bryan), R44GM103389 (Ruan and Bryan), R44GM126676, (Bryan and Chen) and R01GM062154 (Bryan and Orban). The NMR facility is jointly supported by the University of Maryland, the National Institute of Standards and Technology, and a grant from the W. M. Keck Foundation.

We also thank Genisphere LLC (Muro) for technical help with 3DNA®. Mention of commercial products does not imply recommendation or endorsement by NIST.

REFERENCES

1. Vidimar V*, et al.* (2020) An engineered chimeric toxin that cleaves activated mutant and wild-type RAS inhibits tumor growth. *Proc Natl Acad Sci U S A* 117(29):16938-16948.
2. Huang L, Hofer F, Martin GS, & Kim SH (1998) Structural basis for the interaction of Ras with RalGDS. *Nat Struct Biol* 5(6):422-426.
3. Buhrman G, Kumar VS, Cirit M, Haugh JM, & Mattos C (2011) Allosteric modulation of Ras-GTP is linked to signal transduction through RAF kinase. *J Biol Chem* 286(5):3323-3331.
4. Brunger AT*, et al.* (1990) Crystal structure of an active form of RAS protein, a complex of a GTP analog and the HRAS p21 catalytic domain. *Proc Natl Acad Sci U S A* 87(12):4849-4853.
5. Milburn MV*, et al.* (1990) Molecular switch for signal transduction: structural differences between active and inactive forms of protooncogenic ras proteins. *Science* 247(4945):939-945.
6. Gallagher DT, Ruan B, London M, Bryan MA, & Bryan PN (2009) Structure of a switchable subtilisin complexed with substrate and with the activator azide. *Biochemistry* 48 (43):10389-10394.
7. Lu S*, et al.* (2016) Ras Conformational Ensembles, Allostery, and Signaling. *Chem Rev* 116(11):6607-6665.
8. Estell DA*, et al.* (1986) Probing steric and hydrophobic effects on enzyme-substrate interactions by protein engineering. *Science* 233:659-663.
9. Bech LM, Sorensen SB, & Breddam K (1993) Significance of hydrophobic S4-P4 interactions in subtilisin 309 from Bacillus lentus. *Biochemistry* 32(11):2845-2852.
10. Rheinnecker M, Baker G, Eder J, & Fersht AR (1993) Engineering a novel specificity in subtilisin BPN'. *Biochemistry* 32(5):1199-1203.
11. Sorensen SB, Bech LM, Meldal M, & Breddam K (1993) Mutational replacements of the amino acid residues forming the hydrophobic S4 binding pocket of subtilisin 309 from Bacillus lentus. *Biochemistry* 32(35):8994-8999.
12. Rheinnecker M, Eder J, Pandey PS, & Fersht AR (1994) Variants of subtilisin BPN' with altered specificity profiles. *Biochemistry* 33(1):221-225.
13. Takagi H, Maeda T, Ohtsu I, Tsai YC, & Nakamori S (1996) Restriction of substrate specificity of subtilisin E by introduction of a side chain into a conserved glycine residue. *FEBS Lett* 395(2-3):127-132.
14. Takagi H, Ohtsu I, & Nakamori S (1997) Construction of novel subtilisin E with high specificity, activity and productivity through multiple amino acid substitutions. *Protein Eng* 10(9):985-989.
15. DeSantis G, Shang X, & Jones JB (1999) Toward tailoring the specificity of the S1 pocket of subtilisin B. lentus: chemical modification of mutant enzymes as a strategy for removing specificity limitations. *Biochemistry* 38(40):13391-13397.
16. Rockwell NC, Krysan DJ, Komiyama T, & Fuller RS (2002) Precursor processing by kex2/furin proteases. *Chem Rev* 102(12):4525-4548.
17. Ruan B, Fisher KE, Alexander PA, Doroshko V, & Bryan PN (2004) Engineering subtilisin into a fluoride-triggered processing protease useful for one-step protein purification. *Biochemistry* 43(46):14539-14546.
18. Bryan P*, et al.* (1992) Energetics of folding subtilisin BPN'. *Biochemistry* 31(21):4937-4945.

19. Bryan P*, et al.* (1995) Catalysis of a protein folding reaction: mechanistic implications of the 2.0 A structure of the subtilisin-prodomain complex. *Biochemistry* 34(32):10310-10318.
20. Gallagher TD, Gilliland G, Wang L, & Bryan P (1995) The prosegment-subtilisin BPN' complex: crystal structure of a specific foldase. *Structure* 3:907-914.
21. Strausberg SL*, et al.* (1995) Directed evolution of a subtilisin with calcium-independent stability. *Biotechnology (N Y)* 13(7):669-673.
22. Strausberg SL, Ruan B, Fisher KE, Alexander PA, & Bryan PN (2005) Directed coevolution of stability and catalytic activity in calcium-free subtilisin. *Biochemistry* 44(9):3272-3279.
23. Sari N*, et al.* (2007) Hydrogen-deuterium exchange in free and prodomain-complexed subtilisin. *Biochemistry* 46(3):652-658.
24. Ruan B, London V, Fisher KE, Gallagher DT, & Bryan PN (2008) Engineering Substrate Preference in Subtilisin: Structural and Kinetic Analysis of a Specificity Mutant. *Biochemistry*.
25. Hedstrom L (2002) Serine protease mechanism and specificity. *Chem Rev* 102(12):4501-4524.
26. Berger A & Schechter I (1970) Mapping the active site of papain with the aid of peptide substrates and inhibitors. *Philos Trans R Soc Lond B Biol Sci* 257(813):249-264.
27. Bode W, Papamokos E, Musil D, Seemueller U, & Fritz H (1986) Refined 1.2 A crystal structure of the complex formed between subtilisin Carlsberg and the inhibitor eglin c. Molecular structure of eglin and its detailed interaction with subtilisin. *Embo J* 5(4):813-818.
28. McPhalen CA & James MNG (1988) Structural comparison of two serine proteinase-protein inhibitor complexes: Eglin-C-Subtilisin Carlsberg and CI-2-Subtilisin novo. *Biochemistry* 27:6582-6598.
29. Carter P & Wells JA (1987) Engineering enzyme specificity by "substrate-assisted catalysis". 237:394-399.
30. Carter P & Wells JA (1988) Dissecting the catalytic triad of a serine protease. *Nature* 332:564-568.
31. Harpel MR & Hartman FC (1994) Chemical rescue by exogenous amines of a site-directed mutant of ribulose 1,5-bisphosphate carboxylase/oxygenase that lacks a key lysyl residue. *Biochemistry* 33(18):5553-5561.
32. Toney MD & Kirsch JF (1989) Direct Bronsted analysis of the restoration of activity to a mutant enzyme by exogenous amines. *Science* 243(4897):1485-1488.
33. Takahashi E & Wraight CA (2006) Small weak acids reactivate proton transfer in reaction centers from Rhodobacter sphaeroides mutated at AspL210 and AspM17. *J Biol Chem* 281(7):4413-4422.
34. Wells JA & Estell DA (1988) Subtilisin--an enzyme designed to be engineered. *Trends Biochem. Sci.* 13:291-297.
35. Bryan PN (2012) *Engineering Protease Specificity* (Wiley Press, Weinheim).
36. Delano WL (2002) The PyMOL Molecular Graphics System (DeLano Scientific, San Carlos, CA).
37. Radisky ES & Koshland DE, Jr. (2002) A clogged gutter mechanism for protease inhibitors. *Proc Natl Acad Sci U S A* 99(16):10316-10321.
38. Buhrman G, de Serrano V, & Mattos C (2003) Organic solvents order the dynamic switch II in Ras crystals. *Structure* 11(7):747-751.
39. Menetrey J & Cherfils J (1999) Structure of the small G protein Rap2 in a non-catalytic complex with GTP. *Proteins* 37(3):465-473.

40. Araki M, *et al.* (2011) Solution structure of the state 1 conformer of GTP-bound H-Ras protein and distinct dynamic properties between the state 1 and state 2 conformers. *J Biol Chem* 286(45):39644-39653.
41. O'Connor C & Kovrigin EL (2008) Global conformational dynamics in ras. *Biochemistry* 47(39):10244-10246.
42. Vo U, Embrey KJ, Breeze AL, & Golovanov AP (2013) (1)H, (1)(3)C and (1)(5)N resonance assignment for the human K-Ras at physiological pH. *Biomol NMR Assign* 7(2):215-219.
43. Fetics SK, *et al.* (2015) Allosteric effects of the oncogenic RasQ61L mutant on Raf-RBD. *Structure* 23(3):505-516.
44. Buhrman G, *et al.* (2011) Analysis of binding site hot spots on the surface of Ras GTPase. *J Mol Biol* 413(4):773-789.
45. Matsumoto S, *et al.* (2016) Molecular Mechanism for Conformational Dynamics of Ras.GTP Elucidated from In-Situ Structural Transition in Crystal. *Sci Rep* 6:25931.
46. Kraulis PJ, Domaille PJ, Campbell-Burk SL, Van Aken T, & Laue ED (1994) Solution structure and dynamics of Ras p21-GDP determined by heteronuclear three- and four-dimensional NMR spectroscopy. *Biochemistry* 33:3515-3531.
47. Yin G, *et al.* (2017) A KRAS GTPase K104Q Mutant Retains Downstream Signaling by Offsetting Defects in Regulation. *J Biol Chem* 292(11):4446-4456.
48. Lejon S, Frick IM, Bjorck L, Wikstrom M, & Svensson S (2004) Crystal structure and biological implications of a bacterial albumin binding module in complex with human serum albumin. *J Biol Chem* 279(41):42924-42928.
49. Rozak DA, *et al.* (2006) Using offset recombinant polymerase chain reaction to identify functional determinants in a common family of bacterial albumin binding domains. *Biochemistry* 45(10):3263-3271.
50. Schiefner A, Angelov A, Liebl W, & Skerra A (2016) Structural basis for cellulose binding by the type A carbohydrate-binding module 64 of Spirochaeta thermophila. *Proteins* 84(6):855-858.
51. Ikemura H, Takagi H, & Inouye M (1987) Requirement of pro-sequence for the production of active subtilisin E in Escherichia coli. *J Biol Chem* 262(16):7859-7864.
52. Hall BE, Bar-Sagi D, & Nassar N (2002) The structural basis for the transition from Ras-GTP to Ras-GDP. *Proc Natl Acad Sci U S A* 99(19):12138-12142.
53. Killoran RC & Smith MJ (2019) Conformational resolution of nucleotide cycling and effector interactions for multiple small GTPases determined in parallel. *J Biol Chem* 294(25):9937-9948.
54. Zhang B, Zhang Y, Wang Z, & Zheng Y (2000) The role of Mg2+ cofactor in the guanine nucleotide exchange and GTP hydrolysis reactions of Rho family GTP-binding proteins. *J Biol Chem* 275(33):25299-25307.
55. Lu W, *et al.* (2013) The formate/nitrite transporter family of anion channels. *Biol Chem* 394(6):715-727.
56. Stewart V, Lu Y, & Darwin AJ (2002) Periplasmic nitrate reductase (NapABC enzyme) supports anaerobic respiration by Escherichia coli K-12. *J Bacteriol* 184(5):1314-1323.
57. Bone R, Silen JL, & Agard DA (1989) Structural plasticity broadens the specificity of an engineered protease. *Nature* 339(6221):191-195.
58. Stinson BM, Baytshtok V, Schmitz KR, Baker TA, & Sauer RT (2015) Subunit asymmetry and roles of conformational switching in the hexameric AAA+ ring of ClpX. *Nat Struct Mol Biol* 22(5):411-416.
59. Post CB & Ray WJ, Jr. (1995) Reexamination of induced fit as a determinant of substrate specificity in enzymatic reactions. *Biochemistry* 34(49):15881-15885.
60. Phan J, *et al.* (2002) Structural basis for the substrate specificity of tobacco etch virus protease. *J Biol Chem* 277(52):50564-50572.

61. Long AC, Orr DC, Cameron JM, Dunn BM, & Kay J (1989) A consensus sequence for substrate hydrolysis by rhinovirus 3C proteinase. *FEBS Lett* 258(1):75-78.
62. Huang L & Counter CM (2015) Reduced HRAS G12V-Driven Tumorigenesis of Cell Lines Expressing KRAS C118S. *PLoS One* 10(4):e0123918.
63. Lampson BL*, et al.* (2012) Targeting eNOS in pancreatic cancer. *Cancer Res* 72(17):4472-4482.
64. Lim KH, Ancrile BB, Kashatus DF, & Counter CM (2008) Tumour maintenance is mediated by eNOS. *Nature* 452(7187):646-649.
65. Kharitonov VG, Sundquist AR, & Sharma VS (1994) Kinetics of nitric oxide autoxidation in aqueous solution. *J Biol Chem* 269(8):5881-5883.
66. Pahan K, Sheikh FG, Khan M, Namboodiri AM, & Singh I (1998) Sphingomyelinase and ceramide stimulate the expression of inducible nitric-oxide synthase in rat primary astrocytes. *J Biol Chem* 273(5):2591-2600.
67. Ho PK & Hawkins CJ (2005) Mammalian initiator apoptotic caspases. *Febs J* 272(21):5436-5453.
68. Timmer JC & Salvesen GS (2007) Caspase substrates. *Cell Death Differ* 14(1):66-72.
69. Fisher KE, Ruan B, Alexander PA, Wang L, & Bryan PN (2007) Mechanism of the kinetically-controlled folding reaction of subtilisin. *Biochemistry* 46(3):640-651.
70. Ruan B, Hoskins J, & Bryan PN (1999) Rapid Folding of Calcium-Free Subtilisin by a Stabilized Pro-Domain Mutant. *Biochemistry* 38(26):8562-8571.
71. Alexander PA, He Y, Chen Y, Orban J, & Bryan PN (2007) The design and characterization of two proteins with 88% sequence identity but different structure and function. *Proc Natl Acad Sci U S A* 104(29):11963-11968.
72. Poe M, Scolnick EM, & Stein RB (1985) Viral Harvey ras p21 expressed in Escherichia coli purifies as a binary one-to-one complex with GDP. *J Biol Chem* 260(7):3906-3909.
73. Burd CE*, et al.* (2014) Mutation-specific RAS oncogenicity explains NRAS codon 61 selection in melanoma. *Cancer Discov* 4(12):1418-1429.
74. Pear WS, Nolan GP, Scott ML, & Baltimore D (1993) Production of high-titer helper-free retroviruses by transient transfection. *Proc Natl Acad Sci U S A* 90(18):8392-8396.